CHAPTER 5.0 CODE VALIDATION

In this chapter, the numerical approach is validated with simpler experiments, which have been previously reported in the literature. This was done in an effort to compare the solutions obtained with this approach to data from less complex experiments. These "test" problems help provide some insight to the type of behavior that can be expected for the wind tunnel data. The numerical approach was first used to solve the quasi 2-D Navier-Stokes equations with the viscous and heat transfer terms neglected (i.e. Euler's Equation), and the results were compared to a shock tube experiment (Test Number 1). The numerical approach was then used to solve the 2-D N-S equations neglecting viscous terms but accounting for conduction (Test Number 2). The results of Test Number 2 were compared to the results of a benchtest experiment involving a shock propagating through laboratory air and normally impacting a heat flux gage.

5.1 The Governing Equations of Test Number 1

Test Number 1 is applied to the quasi 2-D Navier-Stokes equations with the viscous and heat transfer terms neglected. This system of equations are given as

$$\frac{\partial \rho}{\partial t} + \frac{\partial (\rho v)}{\partial y} = 0 \qquad \text{(continuity)}$$

$$\frac{\partial (\rho u)}{\partial t} + \frac{\partial (\rho u v)}{\partial y} = 0 \qquad \text{(x-momentum)}$$

$$\frac{\partial(\rho v)}{\partial t} + \frac{\partial}{\partial y}\left(\rho v^2 + P\right) = 0 \qquad \text{(y-momentum)}$$

$$\frac{\partial(\rho E)}{\partial t} + \frac{\partial}{\partial y}\left(\left\{\rho E + P\right\} v\right) = 0 \qquad \text{(energy)}$$

This system of equations best represents the shock tube problem, which was performed by Huber et al[30] in the late 1940's. These equations are inviscid, meaning that there are no viscous terms. They are also nonconducting, which means that there are no terms present that represents heat conduction. For this reason, the temperature history in the flow field cannot be accounted for with this set of equations. Before showing the results of this set of calculations, Huber's experimental apparatus will be briefly described.

5.1.1 The Shock Tube Problem

The shock tube used in this experiment is shown in Figure 5.1. The shock tube consisted of a driver section, a trigger, and a driven section. The driver/trigger section was separated from the driven section by a plastic diaphragm. The diaphragm enabled the driver/trigger section to be pressurized prior to the experiment. The different dimensions of the shock tube can be seen in Figure 5.1. The equivalent nondimensional lengths (x/L) are shown on the left of the figure, with the bottom of the shock tube (x/L=0) being designated as the origin.

At the origin (x/L=0), a pressure crystal is placed on the shock tube end cap. This is shown as point B. This pressure crystal is capable of measuring time histories of pressure before, during, and after impact from a normal shock. At a point midway along the driven section (x/L=0.3: shown as point A), a second pressure crystal is installed along the sidewall. This pressure crystal, along with the crystal at the endcap, enables the incident and reflective shock velocities to be measured.

The diaphragm is located at the flange between the trigger and the driven section (x/L=0.6). Once the driver section is pressurized, the trigger punctures the diaphragm. A

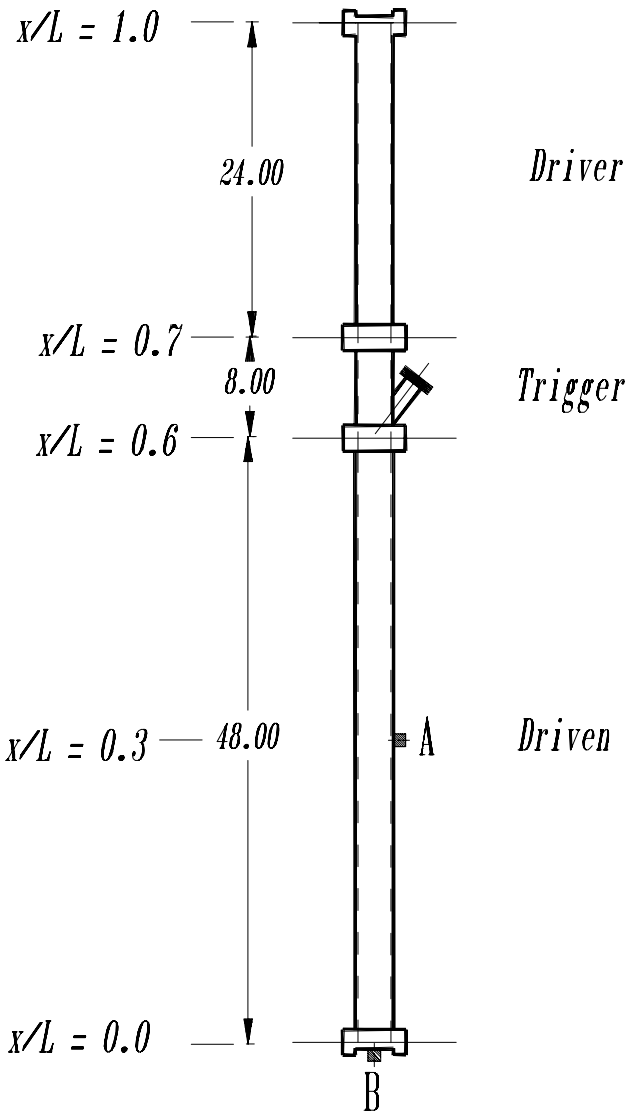

Figure 5.1 **The Shock Tube Apparatus of Huber et al[30]**
(dimensions shown are in inches)

shock of strength 1.4 (pressure ratio across the shock) propagates through the driven section past point A and impacts point B. A reflective shock is produced, which propagates over point A and back to the driver section. In the experiment performed by Huber, a shock propagating towards point B was produced. At the same time, an expansion wave propagating in the opposite direction was observed. This is to be expected and can be reproduced with the right initial conditions. However, it is not of interest in the present research to include the expansion waves for this analysis.

5.1.2 The Initial Conditions

The shock tube relations[31] are used to determine the initial conditions required investigating the shock tube problem (in the absence of expansion waves). Again P/P_{atm} is the desired shock strength to be studied and serves as input to the approach. The initial conditions of the driven section are those corresponding to atmospheric air at 300 K. This corresponds to P_{atm}=1atm, ρ_{atm}=1.1614kg/m^3, and $u_{atm}=v_{atm}=0$ at $x/L \leq 0.6$. The initial conditions of the driver section are shown below, as a function of the shock strength:

$$\frac{\rho_{driver}^{n=0}}{\rho_{atm}^{n=0}} = \frac{1+\frac{\gamma+1}{\gamma-1}\left(\frac{P}{P_{atm}}\right)}{\frac{\gamma+1}{\gamma-1}+\frac{P}{P_{atm}}}$$

$$u_{driver}^{n=0} = 0$$

$$v_{driver}^{n=0} = \frac{a_{atm}^{n=0}}{\gamma}\left(\frac{P}{P_{atm}}-1\right)\left(\frac{\frac{2\gamma}{\gamma+1}}{\frac{P}{P_{atm}}+\frac{\gamma-1}{\gamma+1}}\right)^{\frac{1}{2}}$$

In the above relations, the superscript (n=0) represents the initial conditions. These initial conditions produce a shock in isolation (no expansion waves). They place a shock of desired strength already in motion at a desired position.

5.1.3 Results

The time histories from pressure crystals A and B were measured by Huber and are the source of verification of the code results. Pressure crystal A and B can be seen in Figure 5.1. Figure 5.2 shows the solution to the Euler equations and how it compares to Huber's measured and analytically obtained results at pressure crystal A. The data shows that the shock passes the pressure crystal at x/L=0.3, twice. At first, the incident shock originating from x/L=0.6 passes point A at ~1.55msec. The shock impacts the wall (~3.05msec) and generates a reflected shock, which passes point A at ~4.6msec.

Figure 5.3 shows the pressure history at point B (x/L=0). This figure verifies that the difference in time for shock impact from the Euler equations and Huber's experiment is < 1%. The amplitude of the pressure in the driver section after shock impact (time >3msec) is also ~1%. The strength of the reflected shock is 1.35, which effects the speed of shock propagation (as seen in Figure 5.2 for t~4.6msec). The weaker the reflected shock, the slower the reflected shock propagation velocity. From the times observed in figure 5.2 for the reflected shock, the propagation velocity calculated is ~2% lower than measured. This can be attributed to the ~4% reduction in strength of the reflected shock, and is expected.

5.1.4 Summary

The information gained from test number 1 indicates that applying this approach to MacCormack's method predicts shock speed to within 2% of measurements. The reflected shock strength is predicted to within 4% of measurements. The accuracy of the shock strength directly effects the accuracy of the shock velocity.

The reason for the reduction of the shock strength is due to the fact that the Euler equations (Navier-Stokes with no viscous or heat transfer terms) are being solved in the 2^{nd} mesh system. Roach has previously suggested that a 1^{st} mesh system (grid point on the surface) is

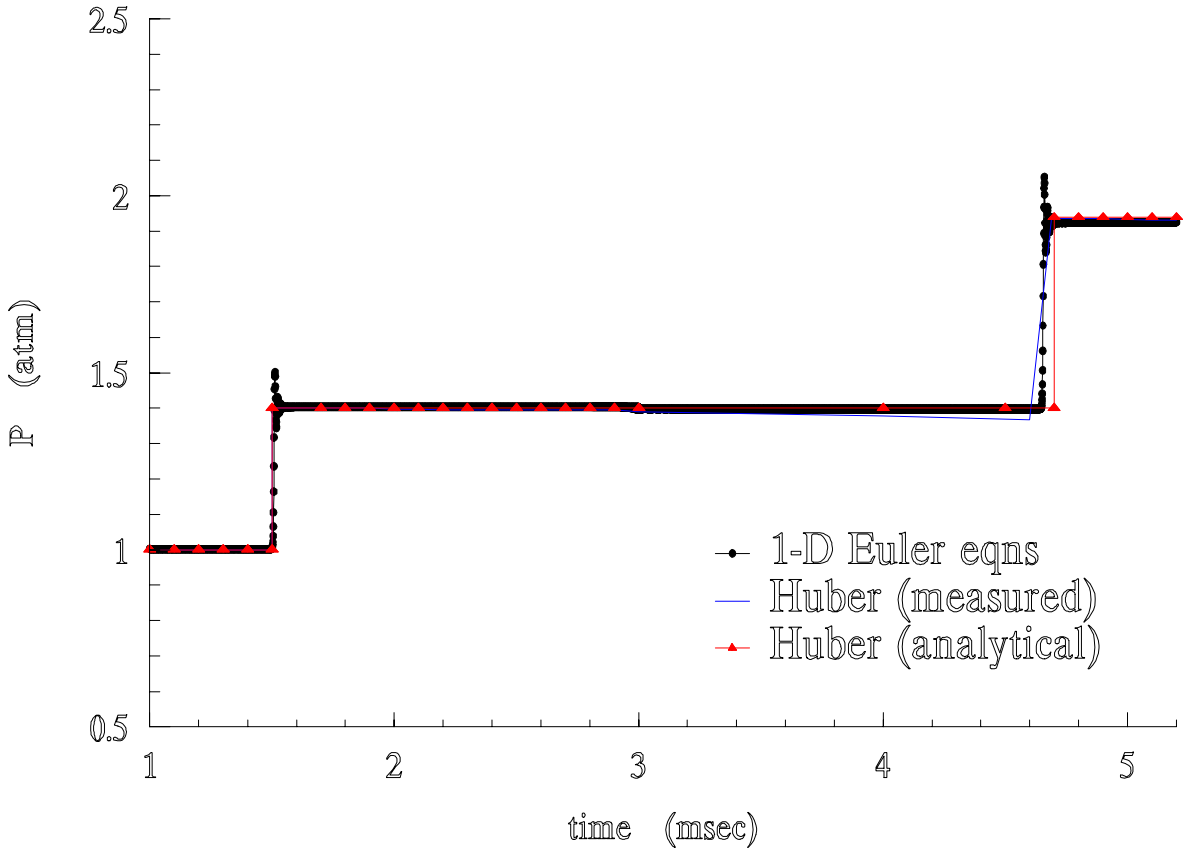

Figure 5.2 Pressure history at crystal A (x/L=0.3)

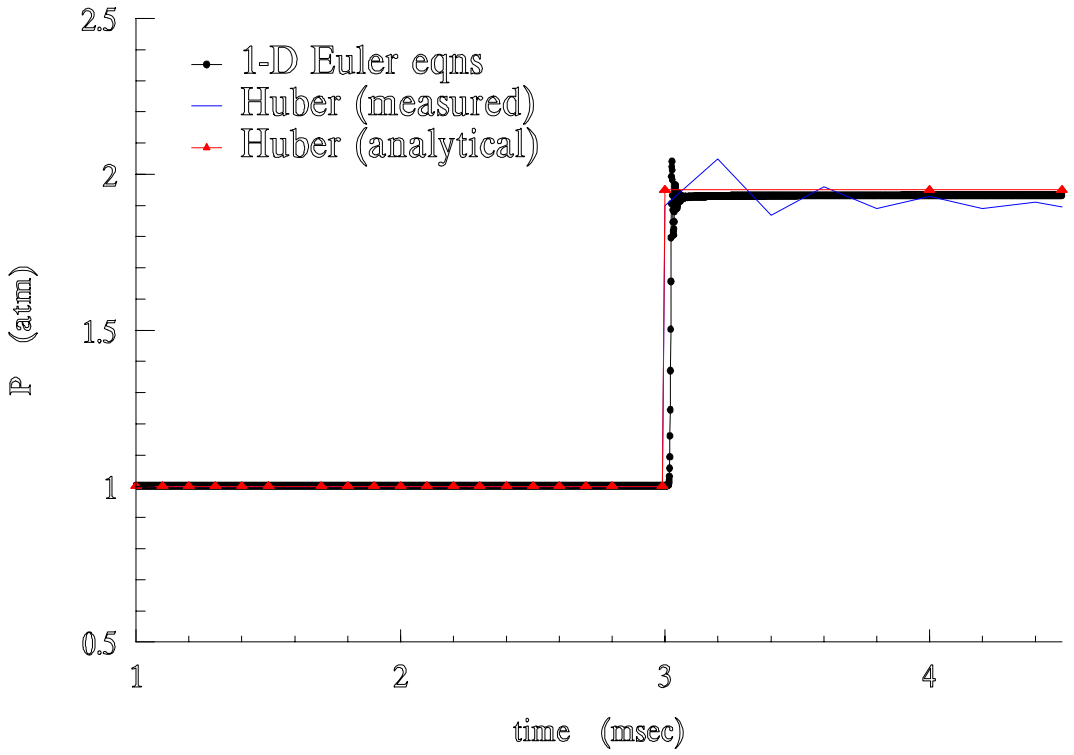

Figure 5.3 Pressure history of crystal B (x/L=0)

best for the Euler equations while the 2nd mesh system (grid points straddling the wall) is best when conduction and/or viscous terms are used. The 2nd mesh system is used throughout this research, therefore an improvement in the accuracy of the reflected shock strength is expected for future results.

5.2 The Governing Equations of Test Number 2

Test Number 2 involves the solution of the quasi 2-D Navier-Stokes equations with the viscous terms neglected, but accounting for a conduction term in the energy equation. This system of equations are defined as

$$\frac{\partial \rho}{\partial t} + \frac{\partial (\rho v)}{\partial y} = 0 \qquad \text{(continuity)}$$

$$\frac{\partial (\rho u)}{\partial t} + \frac{\partial (\rho uv)}{\partial y} = 0 \qquad \text{(x-momentum)}$$

$$\frac{\partial (\rho v)}{\partial t} + \frac{\partial}{\partial y}\left(\rho v^2 + P\right) = 0 \qquad \text{(y-momentum)}$$

$$\frac{\partial (\rho E)}{\partial t} + \frac{\partial}{\partial y}\left(\{\rho E + P\} v - q_y\right) = 0 \qquad \text{(energy)}$$

The solutions to this set of equations are compared to the benchtest experiment, performed by Nix[14]. The inviscid conducting equations are equivalent to the Euler equations, with the addition of a conduction term in the energy equation. The term "inviscid" means there are no viscous terms. The temperature history in the flow field can be accounted for with this set of equations. Before showing the results of this set of calculations, Nix's experimental apparatus will be briefly described.

5.2.1 The Shock Benchtest Apparatus

The shock benchtest apparatus used in this experiment was shown in Figure 5.4. The shock benchtest apparatus utilizes a metal block to hold a shock shaper. The

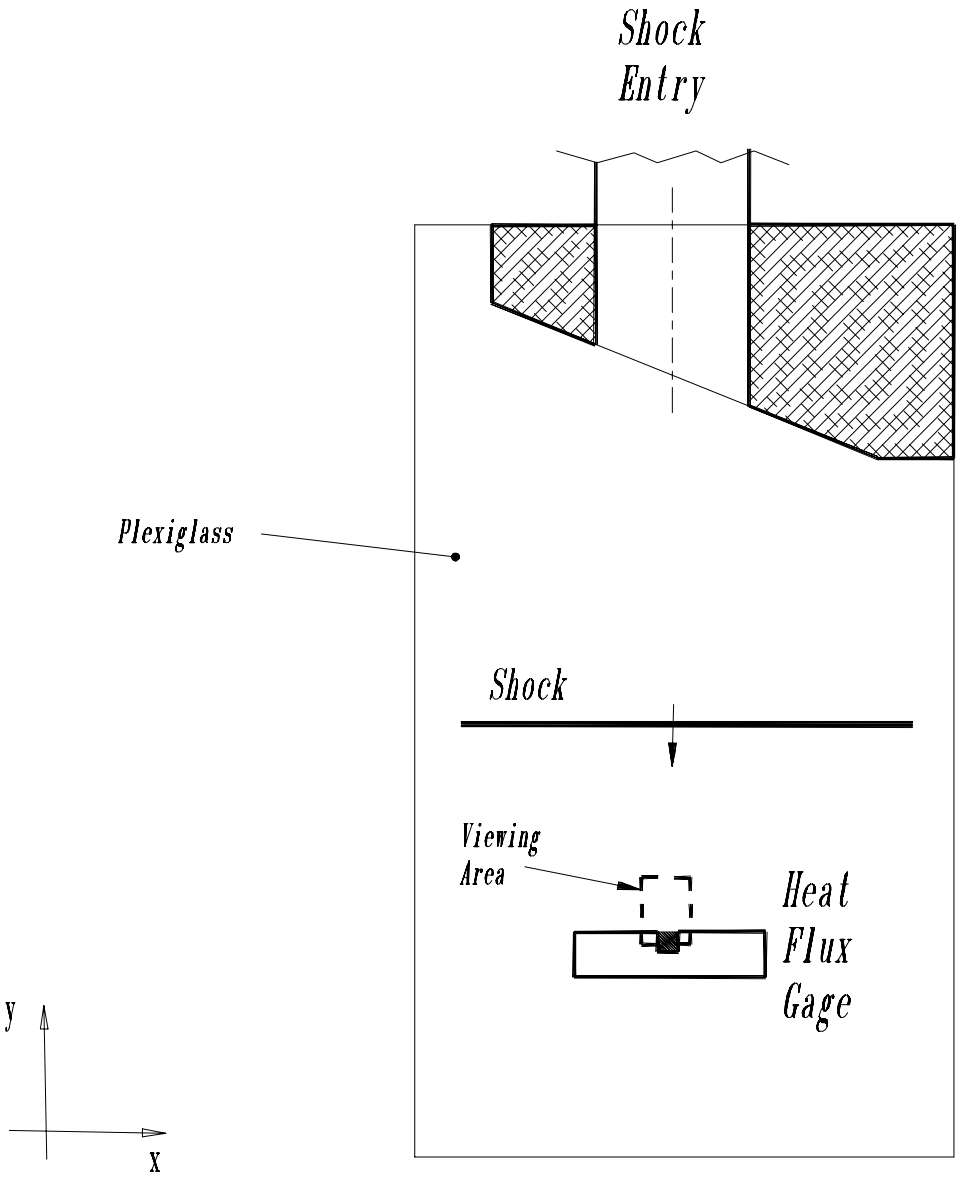

Figure 5.4 The Shock Shaper Benchtest Apparatus used by Nix[14]

shock shaper is connected to the end of a shock tube by means of pressure rated tubing. This allows the shock tube to provide a shock of a predetermined strength to the exit of the shock shaper. The shock shaper is mounted inside of an aluminum block. A large section of 0.5 inch (1.27 cm) Plexiglas is secured to the aluminum block. Approximately 7 inch (1.78 cm) from the end of the shock shaper, a small piece of Plexiglas is secured to the large Plexiglas. The small Plexiglas is used to mount pressure and heat flux gages in a direction perpendicular to the shock motion. As a result, the shock leaving the shaper will eventually impact the gages normally. The details of this apparatus can be seen in Figure 5.4. The section of interest in Figure 5.4 is a 0.5cm square window, referred to as the "viewing area". It is chosen so that the small Plexiglas mount (containing the heat flux gage) can be treated as a solid wall at the bottom of the viewing area. The shock will propagate from the shock shaper toward the top of the viewing area, strike the wall (and the gages), and reflect back toward the shock shaper. Since the shock impact occurs in such a short period of time, the small Plexiglas surface is assumed to maintain a constant temperature.

As the reflected shock propagates away from the wall, it leaves an induced temperature profile on the air adjacent to the wall. By assuming that the wall has a constant temperature, the gaseous medium can be looked at as a semi-infinite medium. With the constant temperature wall at one boundary, semi-infinite conduction theory[32] applies. The solution of the energy equation applied to a semi-infinite medium produces

$$\frac{T(y,t) - T_{wall}}{T_i - T_{wall}} = erf\left(\frac{y}{2\sqrt{\alpha t}}\right) \qquad [5.1]$$

$$q_y = \frac{k(T_i - T_{wall})}{\sqrt{\pi \alpha t}} \qquad [5.2]$$

where the shaded area adjacent to the wall in figure 5.5 refers to a hot stationary "slug" of gas. All of the thermal properties, such as thermal conductivity (k) and thermal diffusivity (α), are for the air at the wall temperature. In equation 5.1, the temperature history is a

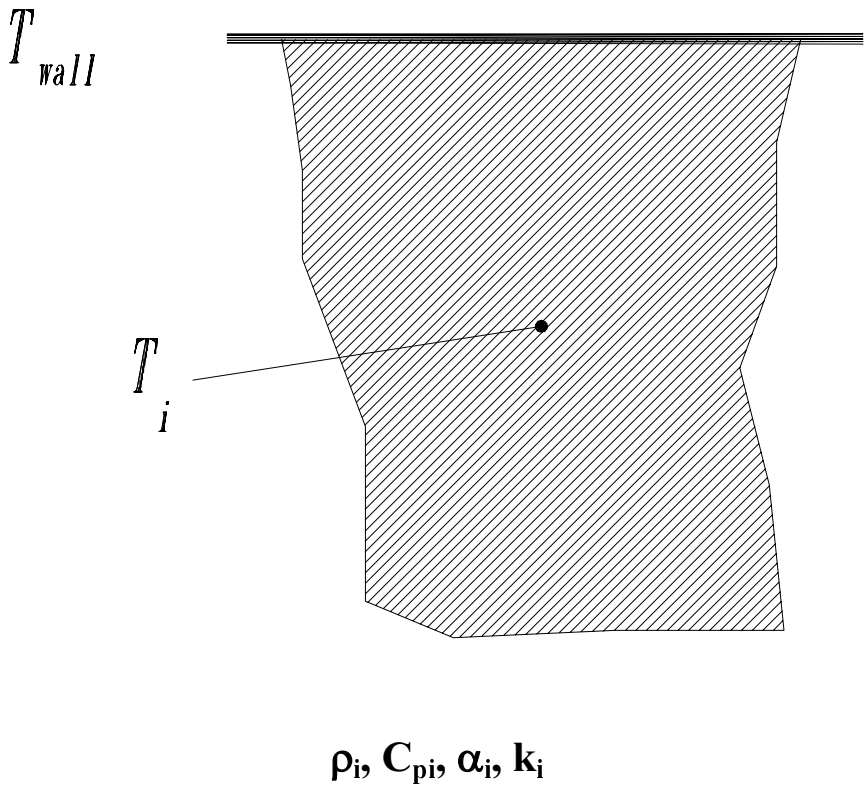

Figure 5.5 Semi-Infinite Conduction Schematic: T_i (is gas temperature) and T_{wall}

function of the difference between the gas and wall temperatures, the thermal diffusivity α, and the absolute distance y away from the wall. Similarly, heat flux (Equation 5.2) is a function of the same parameters with the addition of thermal conductivity k. Equations 5.1 and 5.2 matched the wall heat flux measurements obtain after impact from a shock having a strength = 1.1. It was shown by Nix that semi-infinite conduction reproduces the results of this benchtest experiment adequately. Therefore, the semi-infinite conduction equations (Equations 5.1 and 5.2) can be used to represent the results of the benchtest experiment. They are used for comparison to the solutions to the inviscid conducting governing equations. This system of equations will are solved for a 5mm long viewing window containing a shock (with a pressure ratio of 1.1) and compared to the semi-infinite conduction equations. Throughout this analysis, the amount of artificial viscosity will be varied to determine the optimal amount.

5.2.2 Results

The initial conditions used for this test are identical to those described in Section 5.1.2. The only differences are a smaller viewing area (0.5cm/~0.2inch versus 203cm/80inches) and a weaker shock (1.1 versus 1.4). The length of the window determines the length of time available after shock impact. The smaller window used here will provide only 20μsec of data after shock impact. A weaker shock was used in the experiment of Nix, which is the baseline for comparison. The smaller window also increases the grid density from that used in test number 1. Since the smaller window has been divided into 3000 sections, this yields a grid density of 60 grid points per 0.1mm.

The initial location of the shock is 0.3cm away from the wall. This corresponds to an initial location of x/L=0.4, just as in step 1. Figure 5.6(a-d) shows the incident shock (pressure fields) propagating toward the Plexiglas wall, located at y=0. Figure 5.6a shows the entire flow field as the shock approaches the wall. Figures 5.6 b, c, and d magnify the shock region so the effects of varying the artificial viscosity (or smoothing constant) can be observed. The artificial viscosity is added explicitly after the completion of each time

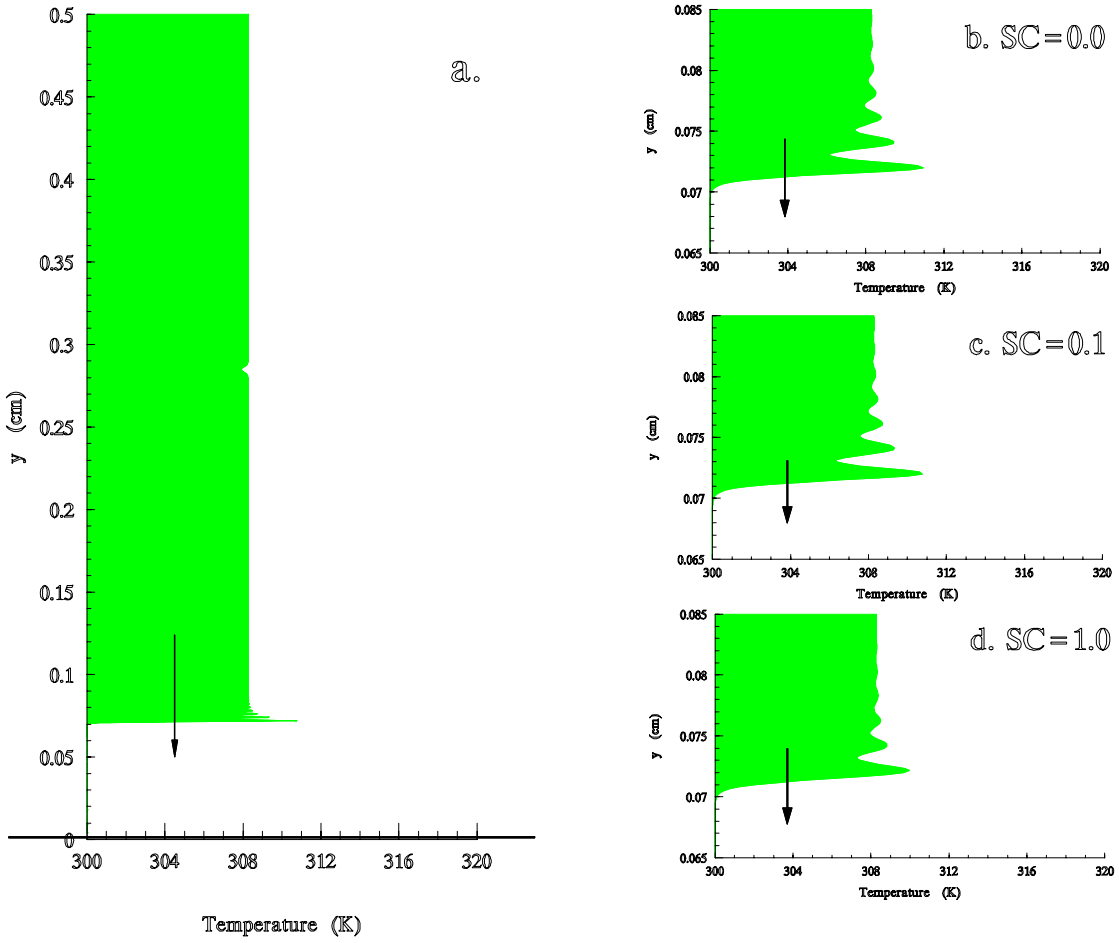

Figure 5.6 **Incident Shock.** (a) Entire temperature field with SC=0.1: 0cm<y<0.5cm, small shock windows: 0.65cm<y<0.85 with artificial constants (b) SC=0.0, (c) SC=0.1 and (d) SC=1.0

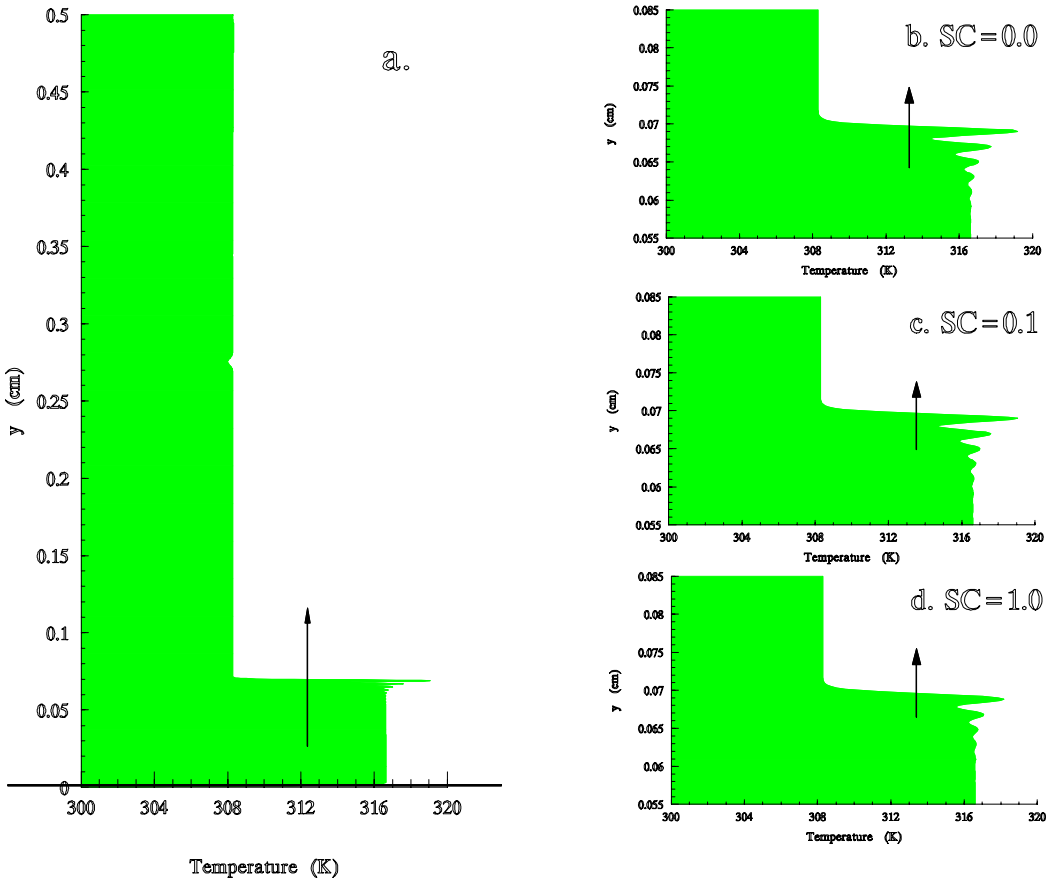

Figure 5.7 **Reflected Shock** .(a) Entire temperature field with SC=0.1: 0cm<y<0.5cm, small shock windows: 0.65cm<y<0.85 with artificial constants (b) SC=0.0, (c) SC=0.1 and (d) SC=1.0

step. This is discussed in detail in Appendix B. It has been recommended by MacCormack that the smoothing constant be in the range of 0.0 to 0.5. The purpose of this smoothing is to reduce the spurious oscillations generated by MacCormack's method. A reduction in the amplitude of oscillation can be seen with increasing smoothing constant, but it is minimal. For the sake of this research, these oscillations will be considered acceptable. In the future, methods that do not produce oscillations should be used. For now, the goal is to evaluate the quasi 2-D approach to see if it is worthwhile to adopt for future unsteady impacting shock analysis.

Similar trends regarding the reflected shock can be seen in Figure 5.7a, b, c, and d. The resulting temperature profiles generated at the wall were magnified and are shown in Figures 5.8, 5.9, and 5.10 (with varying ***S***moothing ***C***onstant). These figures show the transient temperature histories after the shock has impacted the wall, and the generated shock reflection propagates away from the wall. As the shock reflection propagates away from the wall, it leaves a stagnant slug of gas (at 317 K) adjacent to the wall. Figures 5.8, 5.9, and 5.10 show the resulting temperature profiles in a 0.005cm region adjacent to the wall. The symbols shown in the graphs represent the profiles obtained from the solution of the quasi 2-D inviscid conducting version of the governing equations. The lines represent the semi-infinite conduction solutions (Equations 5.1 and 5.2), with a constant temperature wall boundary condition.

Figure 5.8 shows the comparison between the quasi 2-D approach and semi-infinite conduction with no artificial viscosity (SC=0.0). The time intervals are 2, 4, 6, 8, and 10μsec after shock impact. Agreement can be seen for 2 and 4μsec. After 4μsec, the "quasi" 2-D results start to lag behind the semi-infinite solution.

Figure 5.9 shows a comparison between the quasi 2-D approach and semi-infinite conduction with minimal artificial viscosity (SC=0.1). Agreement is observed at all of the time intervals (from 2-10μsec). With increasing time step intervals (>10μsec), the change in the temperature profiles decreases. These transient temperature profiles are appear to adequately model semi-infinite conduction.

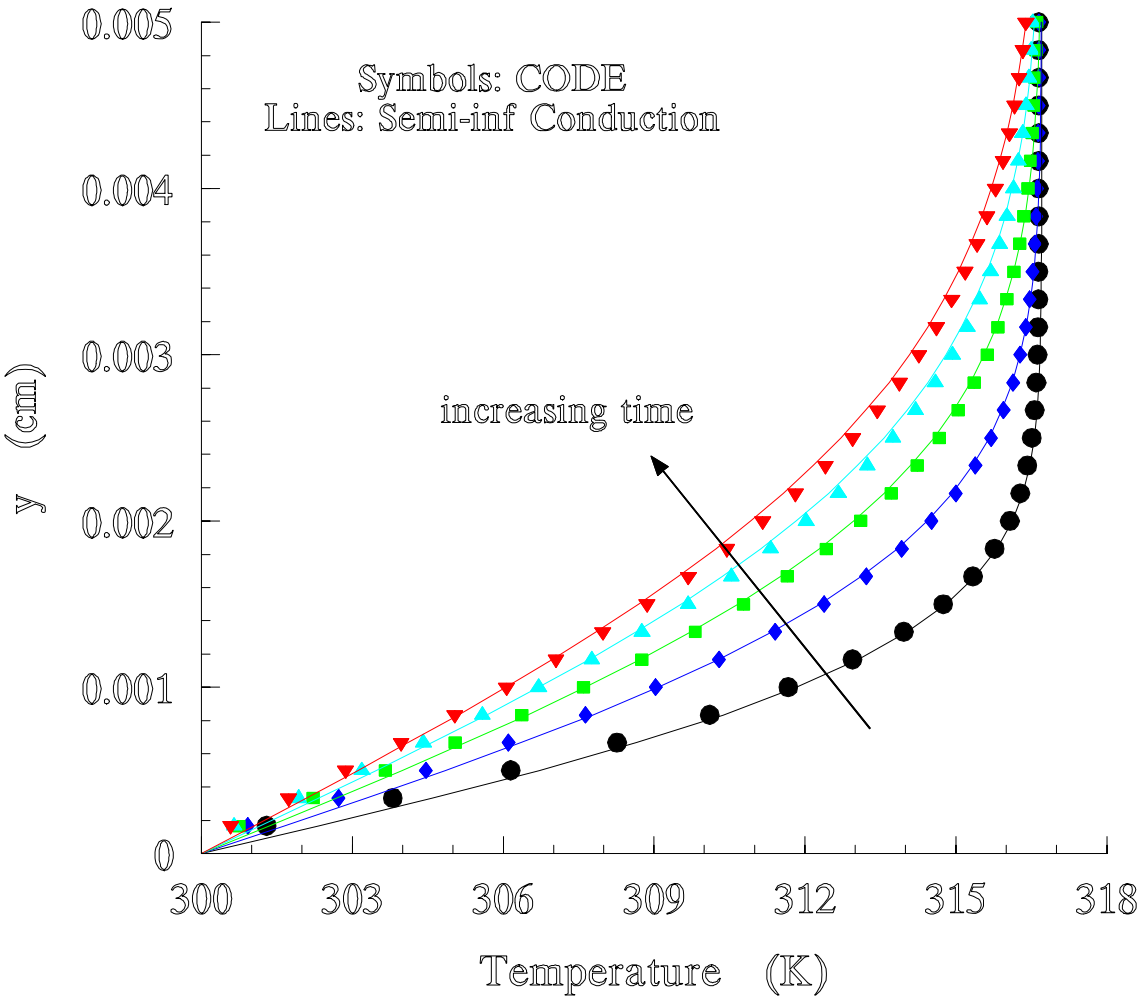

Figure 5.8 Temperature profiles within 0.005cm region adjacent to wall: SC=0.0

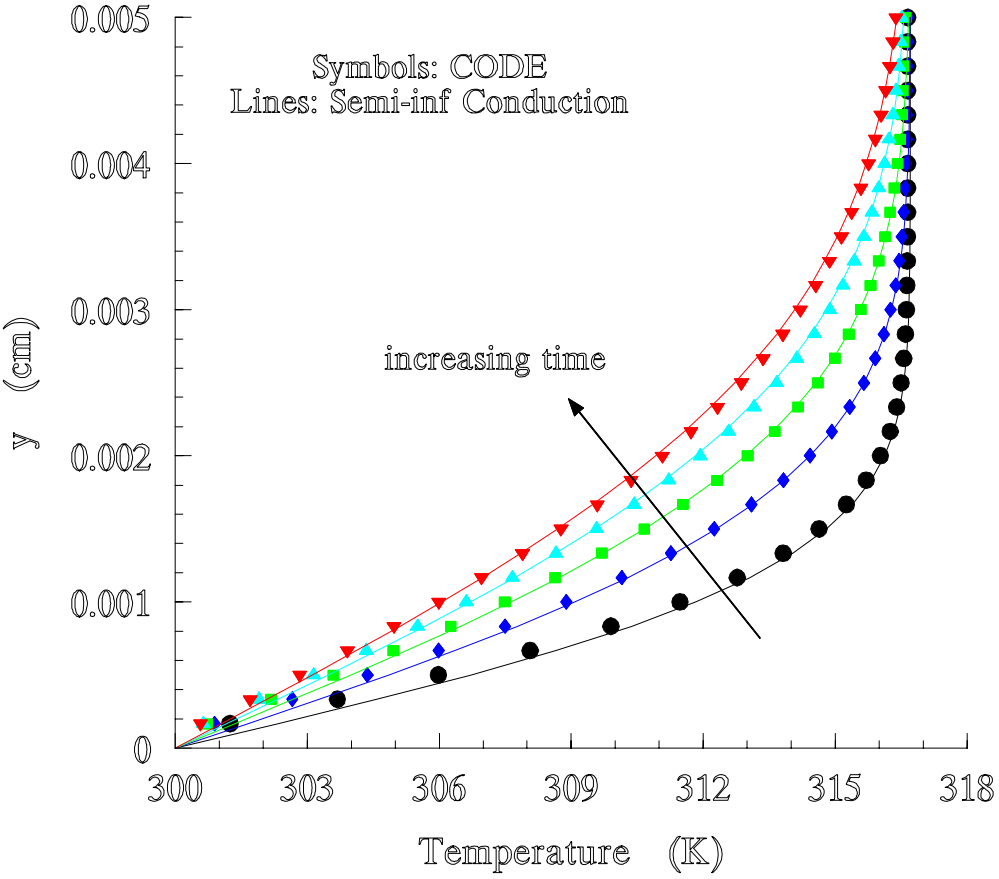

Figure 5.9 Temperature profiles within 0.005cm region adjacent to wall: SC=0.1

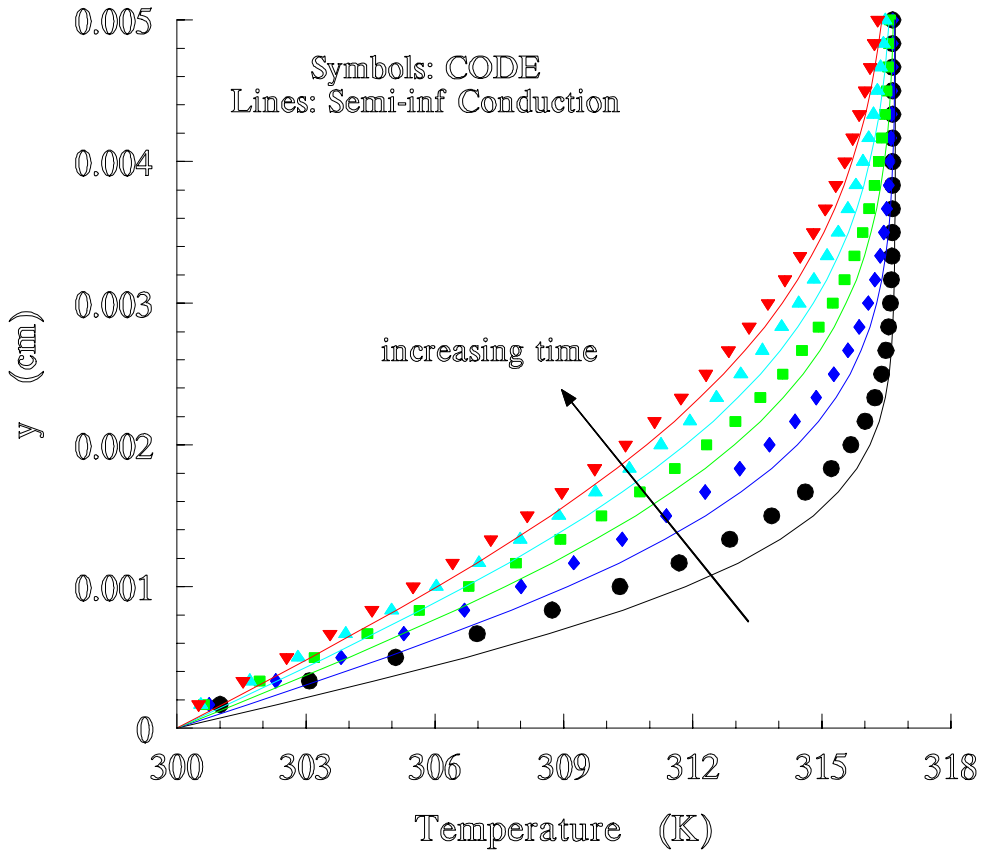

Figure 5.10 Temperature profiles within 0.005cm region adjacent to wall: SC=1.0

Figure 5.10 shows the comparison of the quasi 2-D approach and semi-infinite conduction with excessive artificial viscosity (SC=1.0). The quasi 2-D results are becoming increasingly smeared. This suggests that the temperature gradients are less than those predicted by semi-infinite conduction. These results are consistent with the recommendation of MacCormack regarding artificial smoothing. Smearing of the temperature profiles occurs if excessive artificial viscosity is used (SC>0.5). However, even with excessive artificial viscosity, the spurious oscillations at the discontinuity have not been eliminated. This is a limitation of MacCormack's method. Since the oscillations cannot be eliminated without sacrificing the accuracy of the temperature profiles at the wall, they will be tolerated for the sake of evaluating this approach.

As stated earlier, the initial shock location is 0.3cm away from the wall. The stagnant gas ahead of the shock is 300 K, which suggest a speed of sound a ($\sqrt{\gamma RT}$) of 347.2m/s. The shock has a strength of 1.1 which, from the normal shock tables, should have a Mach number of 1.04. This indicates that the shock should be propagating at a velocity of 361m/s and the wall is 0.3cm away. The shock should impact the wall at 8.3μsec. This can be verified by looking at the heat flux time history at the wall, shown in figure 5.11. In this figure, the oscillations generated at the discontinuity materialize in the heat flux signal. Increasing the artificial viscosity (Smoothing Constant) reduces the amplitude of the peak, which is seen at 8.3μsec. However, it has already been determined that excessive artificial viscosity contaminates the solution. The heat flux results from the quasi 2-D approach (with SC=0.1) matches the semi-infinite conduction solution nicely. For now, the oscillations will be considered tolerable since the true interest of this research involves the surface temperature gradients. Figure 5.12 confirms that the calculated heat transfer resulting from this approach agrees (within reason) with the semi-infinite conduction results. Increasing time indicates that the "steady state" level (time>20μsec) is no greater than 2% of that predicted from semi-infinite conduction. This is reasonable for the 2-D approach and warrants further study.

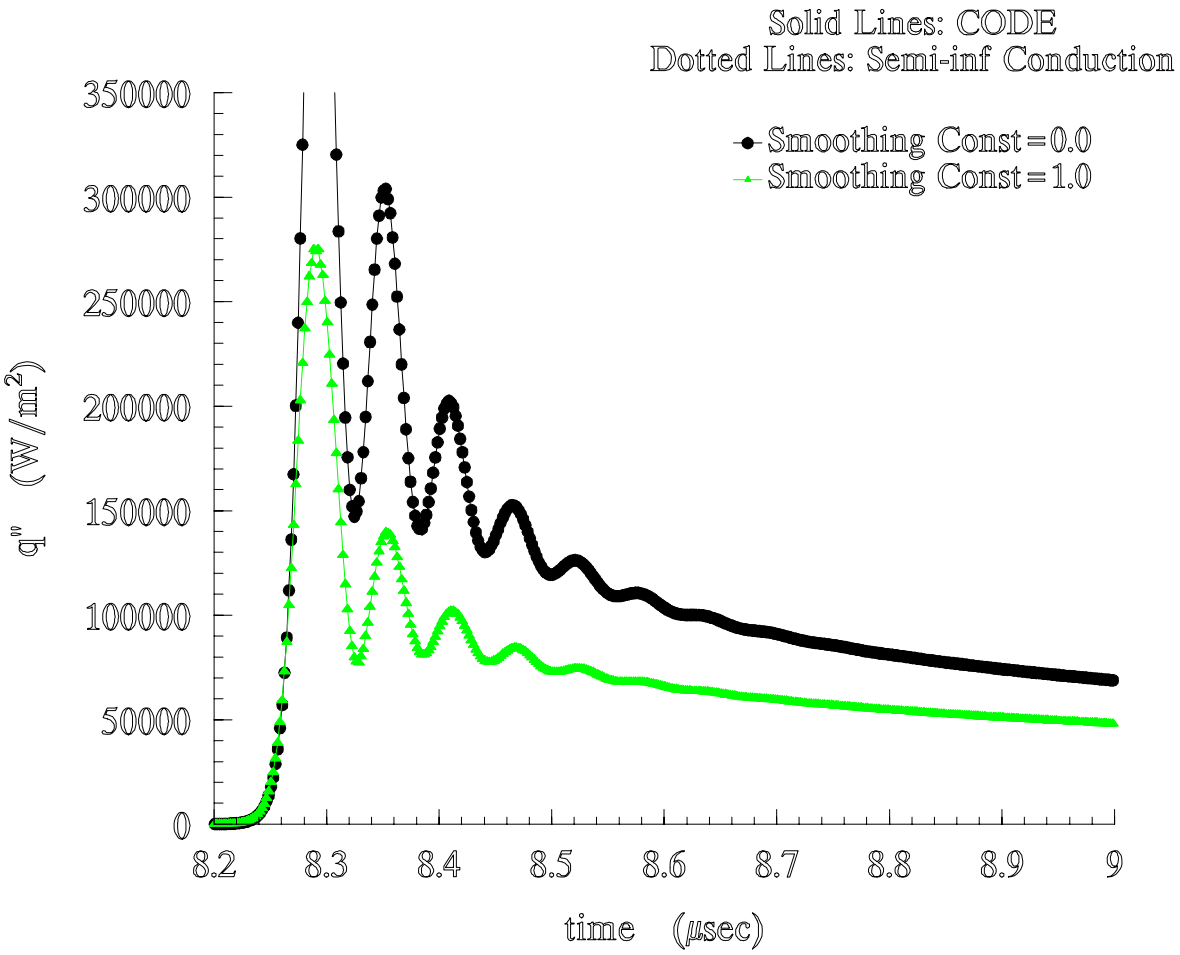

Figure 5.11 Wall heat flux (varying SC): time of impact

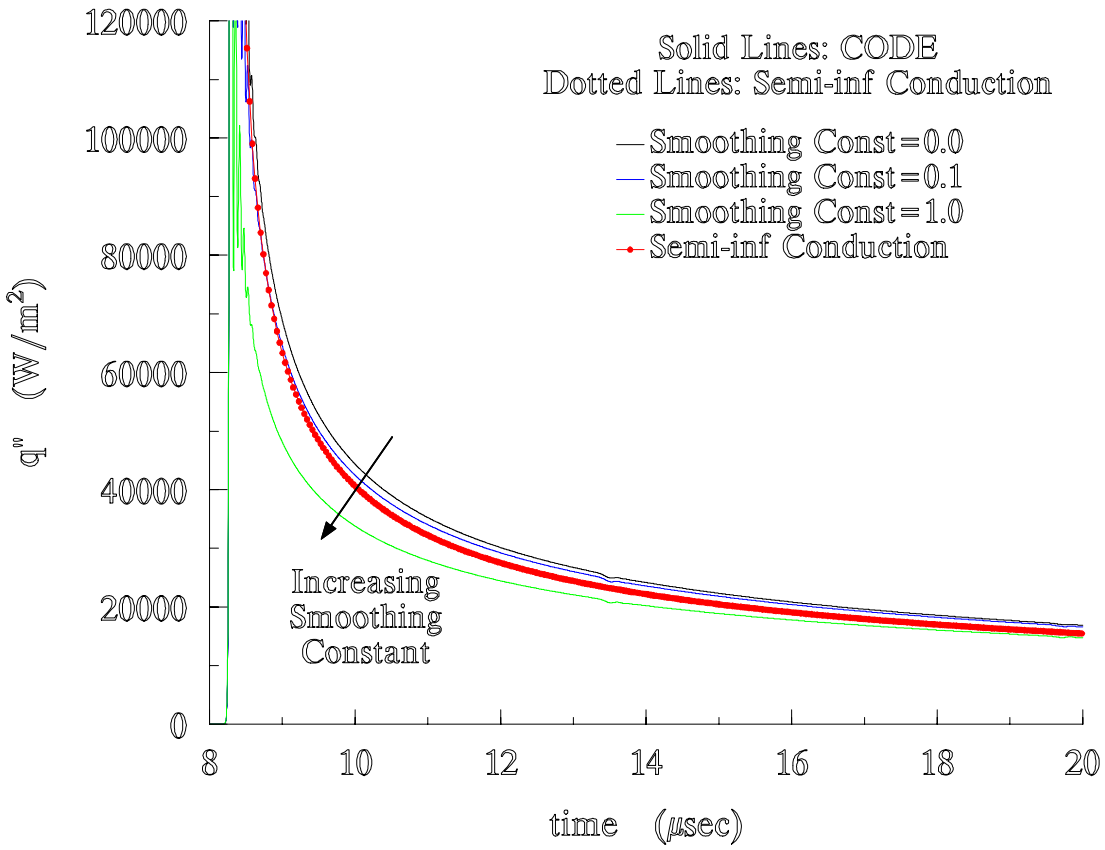

Figure 5.12 Wall heat flux (varying SC) versus semi-infinite conduction

5.2.3 Summary

The information gained from this test condition indicated that artificial viscosity could not totally remove the spurious oscillations at the discontinuity without contaminating the temperature profiles at the wall, which is the area of interest. Tolerating the oscillations at the discontinuity generated by MacCormack's method suggests that minimal artificial viscosity produces solutions at the wall within 2% of semi-infinite conduction (which matched the experimental benchtest data). It is concluded that the quasi 2-D approach reasonably agrees with experimental benchtest data if minimal artificial viscosity is used.

The results of this test have confirmed Roach's recommendation for the 2nd mesh boundary condition for the inviscid conducting system of equations. The calculated incident and reflected shock waves had the same pressure ratio, as expected. The errors of reflected shock propagation strength and speed seen in test number 1, were not seen in test number 2. They are not expected in test number 3. The same (if not better) accuracy is expected for the test number 3, which will be shown in Chapter 6. The results (and errors) shown in this chapter are considered minimal and do not represent a problem.